Journal of Non-Crystalline Solids 358 (2012) 3234–3242

Non-isothermal sinter-crystallization of jagged Li_2O–Al_2O_3–SiO_2 glass and simulation using a modified form of the *Clusters* model

Viviane O. Soares [a,*], Raphael C.V.M. Reis [a,1], Edgar D. Zanotto [a,1], Maria J. Pascual [b,2], Alicia Durán [b,2]

[a] *Vitreous Materials Laboratory, Department of Materials Engineering, Federal University of São Carlos, São Carlos 13565-905, SP, Brazil*
[b] *Instituto de Cerámica y Vidrio (CSIC), C/Kelsen 5, Campus de Cantoblanco, 28049 Madrid, Spain*

ARTICLE INFO

Article history:
Received 22 June 2012
Received in revised form 31 August 2012
Available online 5 October 2012

Keywords:
Sintering;
Viscosity;
Crystallization;
Clusters model;
Glass-ceramic

ABSTRACT

We have tested a modified form of the *Clusters* model of sintering for the complex case of non-isothermal sintering with concurrent crystallization of a multicomponent lithium aluminum silicate (LAS) glass having a broad size distribution of jagged particles. We compared experimental and simulated densification data using a constant heating rate. Only one adjustable parameter was used: the particle shape factor (K_s). We discuss the results in light of some complicating factors, such as temperature gradients within the powder compacts and compositional shifts of the residual glass matrix due to crystallization, which lead to changes of viscosity. The modified *Clusters* model accurately predicted the temperature dependence of densification and the final (saturation) density of the glass particle compacts.

1. Introduction

Glass-ceramics (GCs) based on the Li_2O–Al_2O_3–SiO_2(LAS) system have been extensively investigated because of their low, zero or even negative thermal expansion coefficient (TEC), which gives them excellent thermal shock resistance properties. These materials also have high chemical durability and attractive esthetics [1,2]. LAS GCs were among the first GCs to be developed and are the most important commercial glass-ceramic family. The main products made from these GCs are cooktop panels, cookware, stove windows and precision parts [3,4].

The microstructure of these low expansion GCs is based on a mixture of β-quartz solid solution crystals (β-quartz$_{ss}$) or keatite solid solution crystals, that have a negative volume expansion, mixed with a residual glassy phase that has a small positive volume expansion. GCs can be designed to have a near zero coefficient of thermal expansion by balancing the ratio of these phases [5].

GCs are normally produced by controlled crystallization of certain glasses, which usually involves a two-stage heat treatment: nucleation and crystal growth. In the nucleation stage, a plethora of small nuclei precipitates in the interior of the parent glass. After stable nuclei have formed, crystallization proceeds by the growth of the crystalline phases at higher temperatures [5]. Nucleating agents, such as certain oxides, noble metals and sulfides or fluorides, are normally added to the base glass to promote internal nucleation [6,7]. The most frequently used nucleating agents for LAS GCs are TiO_2 and ZrO_2, used separately or mixed, which is reportedly more efficient than the same amount of either individual component [8,9].

Alternatively, GCs can be produced by sintering glass particle compacts followed by simultaneous or subsequent crystallization [10,11]. This process allows the fabrication of complex shapes using a variety of ceramic forming techniques, *e.g.*, dry pressing, slip casting, tape casting, extrusion and injection molding. One advantage of this method is that sintered GCs do not need nucleating agents because the glass particle surfaces normally have enough defects or solid impurities to catalyze crystallization. However, most crystallizable glass powders are difficult to sinter because the large surface area for nucleation [12] and the premature surface crystallization of the glass particles hamper effective sintering by viscous flow, which is necessary to achieve full density [13]. While the traditional thermal treatment of internally nucleated GCs is well-established in industrial manufacturing [4,14], optimizing sintered GCs for commercial production is still an on-going process.

Little work has been performed on the sintering of LAS-based glasses. Most of these sintering studies started with stoichiometric β-spodumene (Li_2O–Al_2O_3–$4SiO_2$) glass and introduced other oxides that purportedly acted as crystallization inhibitors and/or sintering aids to improve sinterability.

For example, Knickerbocker et al. [15] demonstrated that a glass made from the β-spodumene stoichiometric composition does not sinter well. They evaluated the effect of various oxides on the sintering ability of such materials. The average particle size was between 3.0 and 3.3 μm. They reported that adding 3 wt.% B_2O_3 or

* Corresponding author. Tel.: +55 16 3351 8556; fax: +55 16 3361 5404.
E-mail address: soares.v.o@gmail.com (V.O. Soares).
URL's: http://lamav.weebly.com (V.O. Soares), http://lamav.weebly.com (R.C.V.M. Reis), http://lamav.weebly.com (E.D. Zanotto).
[1] Tel.: +55 16 3351 8556; fax: +55 16 3361 5404.
[2] Tel.: +34 91 7355840; fax: +34 91 7355843.

0022-3093/$ – see front matter © 2012 Elsevier B.V. All rights reserved.
http://dx.doi.org/10.1016/j.jnoncrysol.2012.09.010

P_2O_5 enhanced the material's densification. Nevertheless, the maximum relative density achieved (saturation density) was only approximately 90%.

Sung [16] added small quantities of B_2O_3 and TiO_2 in a stoichiometric β-spodumene glass to obtain LAS GCs with a relative density of approximately 93%. The glass particles were ranged from 5 to 10 μm. The samples were prepared by hot-pressing using a heating rate of 30 °C/min. They reported that adding 2.8 wt.% B_2O_3 plus 3.7 wt.% TiO_2 resulted in the same degree of sintering compared to a composition containing only 3 wt.% B_2O_3[17] (relative density ~93%). However, GCs with TiO_2 showed a slightly lower flexural strength (25 MPa) than those without TiO_2 (32 MPa), although both values are quite low.

Wang et al. [18,19] investigated the effects of TiO_2 additions on the sintering ability of β-spodumene precursor powders prepared by a sol–gel method. The average particle size was not specified by the authors. They found that TiO_2 increased the crystallization temperature and improved sintering. But a relative density of only 70% was obtained for samples with 5 wt.% TiO_2. They observed that precipitates of TiO_2 were segregated and agglomerated at the grain boundaries of the β-spodumene crystalline grains.

The sinterability of two commercial LAS compositions – Ceran® and Robax® – was evaluated by Guedes et al. [20]. The average particle size of glass powders were 1.79 μm for Robax® and 1.66 μm for Ceran®. They demonstrated that both compositions only partially sinter. These commercial compositions contain a significant amount of nucleating agents, which promote crystallization and thus hinder the sintering process. Ceran® and Robax® achieved only 86% and 78% of their theoretical material densities, respectively. Ceran® achieved higher densification levels due to the higher amount of coloring agents present in the base glass, which retarded crystallization during the sintering treatment.

A nanocrystalline LAS GCs with 99% relative density was obtained by Riello et al. [21] using spark plasma sintering under pressure. The powder was prepared by a sol–gel route, but the average particle size was not specified by the authors. A heating rate of 200 °C/min was used, the sintering temperature was 900 °C and a uniaxial pressure of 53 MPa was applied for 5 min. The resulting sample presented a maximum of 45 wt.% of crystalline phase.

Suzdal'tsev et al. [22,23] reported that the sintering of a LAS-based glass could be accelerated by adding 0.1–0.7 wt.% Cr_2O_3. GCs with only 0.1–0.2% residual porosity were obtained by slip casting the glass powders and then heating them. The particle size distribution ranged from 63 to 500 μm. Although almost full densification was achieved, the TEC of this glass-ceramic was higher than 0.5 ppm $°C^{-1}$.

Therefore, obtaining a dense, low expansion, sintered LAS glass-ceramic is not trivial, as demonstrated by the empirical studies mentioned above. In the past decade, our research group has made several efforts to precisely describe the non-isothermal sintering kinetics of glass powders. The *Clusters* model was proposed by Prado et al. [24,25] to describe the viscous sintering kinetics of glass powders with polydisperse particle sizes that undergo concurrent surface crystallization. This model is based on the two classical sintering stages proposed by Frenkel (F) and Mackenzie–Shuttleworth (MS) by considering sample shrinkage as the sum of the partial shrinkage of several "clusters", each one of them consisting of equally sized particles and showing independent F or MS behavior.

The aim of this work is to test an improved form of the *Clusters* model for a multi-component, non-stoichiometric LAS-based glass with a broad size distribution of jagged particles. We compare simulated densification curves with experimental data for non-isothermal sintering using a constant heating rate and several end temperatures. A new solution for the MS expression is proposed and the equation that describes this stage of sintering in the original *Clusters* model is modified to produce a more coherent form. In this research, we used only one fitting parameter, K_S, which is related to the deviation from the idealized spherical shape of the particles because currently there are no methods to measure or calculate it *a priori*. We also consider temperature gradients within our particle compacts since a thermal lag between the sample surface and its center is unavoidable in non-isothermal sintering. We show that the simulated and experimental curves compare quite well using these modifications.

2. Summary of the supporting theory and the *Clusters* model

The *Clusters* model has been presented in detail in other publications [24–31]; thus, it will only be briefly reviewed here. A modification in the equation for the late stages of non-isothermal sintering with concurrent crystallization – based on the Mackenzie and Shuttleworth model – will also be presented.

2.1. The Frenkel and Mackenzie–Shuttleworth models

The Frenkel model (F) describes the early stage of isotropic sintering of monodisperse spherical particles and is valid for the initial 10% of linear shrinkage [32], *i.e.*, the neck formation stage. When the particles are jagged, an empirical constant, termed the shape factor, K_s, has been proposed and is used to fit the measurements, as shown by Eq. (1).

$$\frac{\Delta L(t)}{L_0} = \frac{3\gamma K_s}{8\eta(T)r}t \tag{1}$$

where L_0 is the original sample length, ΔL is the linear shrinkage after a sintering time t, $\eta(T)$ is the temperature-dependent shear viscosity, γ is the glass-vapor surface energy (whose temperature dependence is very small) and r is the initial particle radius. Jagged particles are known to sinter faster than spherical particles, such that, by definition, $K_s = 1$ for spherical particles, while values ranging from 1.8 to 5 have been reported for jagged particles [24].

If the shrinkage is isotropic and the compact is assumed to be formed by a cubic array of monodisperse particles, then:

$$\rho_F(t) = \frac{\rho_0}{\left[1-\frac{\Delta L(t)}{L_0}\right]^3} \tag{2}$$

where ρ_0 is the relative green density of the compact.

For non-isothermal processes, time can be treated as a temperature-dependent variable, $dt = dT/q$, where q is a constant heating rate. From Eqs. (1) and (2) with $C = 3\gamma K_S/8r$, the sintering rate for a non-isothermal process can be written as:

$$\frac{d\rho_F(T)}{dT} = 3\frac{C{\rho_0}^{-1/3}\rho_F(T)^{4/3}}{q\eta(T)}. \tag{3}$$

By integrating Eq. (3), the densification kinetics for a non-isothermal process is:

$$\rho_F(T) = \rho_0\left(1-\frac{c}{q}\int_{T_0}^{T}\left[\frac{1}{\eta(T')}\right]dT'\right) \tag{4}$$

where T_0 is the temperature in the onset of sintering, generally equal to T_g.

For higher relative densities when the pores are spherical and are isolated in the glass matrix, the Mackenzie–Shuttleworth for an isothermal process, MS model, gives the following densification rate [33]:

$$\frac{d\rho_{MS}(t)}{dt} = \frac{3\gamma}{2a_0\eta(T)}(1-\rho_{MS}(t)) \tag{5}$$

where a_0 is the initial radius of the spherical pores.

For a non-isothermal process and with $C' = \frac{3\gamma}{2a_0}$ the equation becomes:

$$\rho_{MS}(T) = 1-(1-\rho_0)e^{\frac{-C'}{q}\int_{T_{0.8}}^{T}\left[\frac{1}{\eta(T')}\right]dT'} \quad (6)$$

where $T_{0.8}$ is the temperature where $\rho = 0.8$ and the sintering changes from the F to the MS regime, which is explained in details in a following section. The *Clusters* model for non-isothermal sintering was used previously and compared to hot-stage microscopy data in ref. [34].

2.2. Surface crystallization

We assume the simplest case of surface crystallization for powdered glasses: heterogeneous nucleation of semi-spherical crystals from a fixed number of sites per unit area (N_s), which grow on the particles surfaces with a linear growth rate, U(T). The crystals are circular on the surface with a spherical calotte growing inwards the particle's center. In this specific case, the JMAK [35] theory can be used to predict the crystallized surface fraction (α_s) for an infinite surface. For a non-isothermal process, the crystallized surface fraction can be written as a function of temperature:

$$\alpha_S(T) = 1-e^{-\pi\frac{N_S}{q^2}\left(\int_{T_0}^{T} U(T')dT'\right)^2}. \quad (7)$$

Müller et al. [36] reasonably assumed that the densification rate should decrease during the sintering process in proportion to the surface fraction of glass remaining after crystallization. For the case of non-isothermal densification, this can be expressed as:

$$\frac{d\rho_c(T)}{dT} = \frac{d\rho(T)}{dT}(1-\alpha_s(T)) \quad (8)$$

where ρ_c is the relative density of a compact that devitrifies during the sintering process.

2.3. Non-isothermal sintering with concurrent crystallization

The *Clusters* model can be used to predict the densification of a glass powder in the presence of crystallization, by combining the models of F and MS with Eq. (8), proposed by Müller [37,38].

Solving the differential equation formed from Eqs. (3) and (8), one arrives at the Frenkel expression for non-isothermal sintering with surface crystallization:

$$\rho_{c,F}(T) = \frac{\rho_o}{\left[1-\frac{c}{q}\int_{T_0}^{T}\left[\frac{1-\alpha_s(T')}{\eta(T')}\right]dT'\right]^3}. \quad (9)$$

The equation above was used in the original *Clusters* model for non-isothermal sintering proposed by Prado et al. [25,28].

The equation for the MS regime used in this work was obtained by solving the differential Eq. (10), formed by Eqs. (5) and (8). The solution of this equation is Eq. (11) which correctly takes the influence of crystallization on densification into account.

$$\frac{d\rho_{c,MS}(T)}{dT} = \frac{C'}{q\eta(T)}\left(1-\rho_{c,MS}(T)\right)(1-\alpha_s(T)) \quad (10)$$

$$\rho_{c,MS}(T) = 1-(1-\rho_0)e^{\frac{-c'}{q}\int_{T_{0.8}}^{T}\left[\frac{\left(1-\alpha_s(T')\right)}{\eta(T')}\right]dT'}. \quad (11)$$

This solution differs from the one obtained by Prado et al. [25,28] since in their work Eq. (5) was first solved for the case in which no crystallization takes place and then the influence of crystallization (Eq. (8)) was applied to this result, so that the sintering rate would equal the sintering rate of the non-crystallizing case multiplied by the vitreous surface fraction, $(1-\alpha_S(t))$.

Eq. (11), on the other hand, has a more accurate physical meaning, since both dependencies of the sintering rate on $\rho(t)$ and $\alpha_S(t)$ are considered simultaneously — so, in effect, the lower sintering rate caused by the presence of surface crystallization slows the densification, $\rho(t)$, and this effect is correctly taken into account. The most notable difference between the models is the prediction of an increased saturation density in comparison to the original model, the magnitude of which depends on the rate of crystallization *versus* the rate of sintering.

2.4. The Clusters model

The *Clusters* model proposed by Prado et al. [25] describes the sintering of a glass powder compact with a certain particle size distribution. It assumes that small particles fill up the interstitial spaces between the large ones, forming small clusters that sinter faster than their larger neighbors. Each cluster individually reaches the stages of sintering described by the F and MS models. The density of the compact is calculated by the sum of the densities of each cluster multiplied by its corresponding volumetric fraction. Considering a compact with an initial (green) relative density of 0.6, the Frenkel stage of sintering is valid up to a relative density of approximately 0.8. After that, the Mackenzie–Shuttleworth equation is used to calculate the cluster's density. The value of 0.8 has been shown to coincide with the maximum experimental sintering rate for a powder compact, which is expected to happen in the transition between the models [39].

Thus, for a polydisperse compact with a volume fraction ν_r of particles with radius r, the following expression for the densification kinetics was proposed:

$$\rho(T) = \frac{\sum_r\left[\rho_{c,F}(r,T)\cdot\theta_F(T_{0.8}-T)\xi_r + \rho_{c,MS}(r,T).\theta_{MS}(T-T_{0.8})\right]\cdot\nu_r}{\sum_r[\theta_F(T_{0.8}-T)\xi_r + \theta_{MS}(T-T_{0.8})]\cdot\nu_r} \quad (12)$$

where ξ_r is defined as the "neck-forming ability" of each particle of size r, calculated from the particle size distribution and reflects the effect of the contact between particles of different sizes on the sintering kinetics. In this work we considered $\xi_r = 1$, which in effect disregard any interaction between particles of different sizes during the F regime and thus each particle cluster sinters independently. The density of the sample was calculated by the average of the densities of each cluster weighted by its volume fraction in the particle size distribution. Although there must to be some interaction between particles of different sizes, this effect and the effect of the non-spherical particle shape are mixed and it is not trivial to decouple them. Therefore, in this work both effects are considered using the adjustable shape factor, K_s.

The subscript F indicates sintering in the Frenkel stage and the subscript MS indicates the Mackenzie–Shuttleworth stage. The transition between stages happens for each cluster independently at a temperature of $T_{0.8}$, which is the temperature where a given cluster reaches the relative density of 0.8. For each cluster, the transition from the F regime to the MS regime was made using a step function, which has values of 1 and 0 for positive and negative arguments, respectively. As a result, $\theta_F(T_{0.8}-T) = 1$ and $\theta_{MS}(T-T_{0.8}) = 0$ for temperatures below $T_{0.8}$ and they invert values for temperatures above $T_{0.8}$.

Eqs. (9), (11) and (12) are used in this paper.

3. Experimental procedure

A LAS glass within the chemical composition range (mol%): 60–70 SiO_2; 10–20 Al_2O_3; 5–10 Li_2O; 1–4 MgO and other minor oxides, was obtained from analytical-grade chemicals. The mixture of precursor powders was melted in a platinum crucible at 1600 °C for 3 h in an electrical furnace in air. The melt was quenched into water and the small (~2 mm) pieces of glass obtained were crushed in a planetary ball mill (Fritsch Pulverisette) using an agate jar and agate balls of 20 mm in diameter. Two distinct size distributions were obtained, using the milling conditions: 450 rpm for 60 min and 450 rpm for 60 min followed by 550 rpm for 30 min. These two size distributions were mixed at a weight ratio of 2:3 to improve the particle packing and, consequently, to maximize the green density of the compacts; as determined by the Alfred model for particle packing [40,41] and experimentally in [42].

Several parameters were independently measured to perform the computer simulations using the *Clusters* model: particle size distribution, glass transition temperature (T_g), green density (ρ_0), glass density (ρ_g), viscosity ($\eta(T)$), crystal growth rate ($U(T)$), total number of surface nucleation sites per unit area (N_s) and the sample's relative density as a function of end temperature ($\rho(T)$). The glass-vapor surface energy (γ) was estimated from the glass' chemical composition using the SciGlass™ database.

The particle size distribution was measured by laser scattering using a Horiba LA930 device. DSC analyses were performed using a Netzsch DSC 404 and a heating rate of 10 °C/min.

Small cylinders (diameter 10 mm, height 8 mm) were produced by isostatically pressing the glass powder at 200 MPa for 60 s, using 2 wt.% of a commercial ceramic binder. The samples were then treated at 500 °C for 120 min in an electric furnace to remove the binder. The green density was determined by the geometrical method after removing the binder.

The density of a pore-free monolithic glass sample ($\rho_g = 2.40$ g/cm^3) was measured by a Mettler Toledo AX205 density measurement instrument following Archimedes' principle. Room temperature water was used as the immersion liquid.

The glass-vapor surface energy (γ) was calculated using the SciGlass™ software database following the Priven 2000 method. The γ of silicate glasses only weakly depends on temperature, its variation is in the order of 1 to 2% for each 100 °C [43]. To simplify the calculations and because the temperature dependent values were not available, it was reasonably assumed to be temperature-independent.

The glass viscosity was measured for two temperature intervals: 710 °C to 750 °C and 1200 °C to 1500 °C. Low temperature data were obtained using the penetration method with a 2 mm cylindrical indenter. The sample was prepared by melting approximately 100 g of glass powder in a platinum crucible at 1630 °C for 30 min. The liquid was quenched by pouring it into a 2 cm diameter cylindrical graphite mold and then cutting and polishing a 6 mm thick piece. The high temperature viscosity was determined using the rotation method in a Haake viscometer coupled with a ME 1700 sensor. The rotation procedure was applied for viscosity in the range 10^4–10^2 Pa·s using a high-temperature cylindrical probe of the Searle type at rotation speeds of 1–30 rpm for 10 min, following the International Standard ISO 7884-2. Three measurements were taken at three different rotation speeds for each temperature within this range. The viscosity curve was obtained by fitting the Vogel–Fulcher–Tamman equation [$\log\eta = A + B/(T - T_0)$] to the entire set of data (low- and high-viscosities).

The crystal growth rates, $U(T)$, were measured in bulk samples obtained by melting the glass powder in a platinum crucible at 1600 °C for 30 min and then pouring it in a cylindrical graphite mold, as described previously. Samples were cut into 2 mm slices, ground with SiC abrasive papers and polished with a CeO_2 slurry. The polished samples were heat-treated in air in an electric furnace at the following temperatures: 850 °C, 900 °C, 950 °C and 980 °C for several minutes. Each sample was heat treated only once. The heat treated samples were etched with a 2 vol.% HF solution for 15 s and were then observed under an optical microscope (ZEISS, HP1) coupled to a camera (AXIOCAM-MR5) and image analyzing software (ImageJ). One-half of the maximum length of the ten largest isolated surface crystals (the first nucleated ones) found in a given set of micrographs was taken. The average of these values was considered to be the maximum crystal length (R_{MAX}).

Samples treated at 850 °C, 950 °C and 980 °C were analyzed by X-ray diffraction (XRD) using a Rigaku Ultima IV diffractometer. The diffractograms were recorded using CuKα radiation and were measured in a θ–θ geometry. The 2θ range was scanned from 18° to 28° with a step size of 0.02° in the 2θ scale. The crystalline phases were identified based on a search in the JCPDS-ICDD database.

For the determination of the number of nucleation sites per unit area (N_s), a green compact was fractured to expose the internal glass particles and then sintered at 30 °C/min to 900 °C. This heat treatment was enough for the crystals to grow to about 300 nm and still remain mostly separated from each other. The sample was subsequently etched by immersion in 2 vol.% HF solution for 15 s and coated with a thin layer of gold. A scanning electron microscope (Philips XL 30 FEG) was employed to analyze the partially crystallized surface of the sintered sample. The number of crystals was measured for each micrograph and divided by the considered area using the software ImageJ for image analysis. A total of 22 micrographs (magnification 8000×) were measured.

This method underestimates somewhat the analyzed surface area of the particle compact (and therefore overestimates N_s), since it considers the flat area of the picture and not the real topography of the particles. It can be easily demonstrated that the measured (flat) area of a spherical particle would be only half of its real surface area and for a plane tilted 45° in relation to the plane of view, approximately 71% of the true value. This error was offset by not considering the particles borders or very tilted surfaces in our measurements, since the more tilted the surface is in relation to the plane perpendicular to the view axis, the larger the error. Areas of porosity were not considered either. Therefore, we believe that the actual N_s is not far from the measured one, although, rigorously, it should be treated as an upper bound. Hence the calculated crystallized fraction could be somewhat overestimated.

Two different sintering experiments were conducted: in the first one, the compacts were sintered in air at 28 °C/min to different final temperatures using a tubular furnace (TF). After reaching the desired temperatures, the samples were immediately removed from the furnace and air-quenched to room temperature to preclude any additional sintering and crystallization on the cooling path. The sintered compact densities ($\rho(T)$) were then determined at room temperature by the geometric method.

In a second experiment, a single sample was sintered using a hot stage microscope (HSM) (Misura HSM ODHT — Expert System Solutions) also at a constant rate of 28 °C/min. This second experiment was performed using a smaller sample to minimize thermal gradients, so that the resulting data could be better compared to simulation results. The sample (approximately a cube of about 33 mm^3) was placed on an alumina support and the temperature was measured with a Pt/Rh thermocouple in contact under the alumina support. The heating microscope projected the image of the sample through a quartz window and images of the sample were captured by a video camera every 2 °C. The relative density was calculated using the measured axial and horizontal shrinkages, Eq. (13).

$$\rho(t) = \frac{\rho_0}{\left(1 - \frac{\Delta L_R(t)}{L_{Ro}}\right)^2 \left(1 - \frac{\Delta L_A(t)}{L_{Ao}}\right)}, \tag{13}$$

where the subscripts R and A indicates horizontal and axial (vertical) shrinkages.

Scanning electron microscopy (SEM, Phillips TMP) with a secondary electron (SE) detector was employed to observe the microstructure of polished and etched (HF immersion) transversal sections of a sample sintered up to 1000 °C.

4. Results

4.1. Glass and powder characterization

The particle size distribution of the glass powder exhibited a bimodal distribution, with maxima of approximately 0.6 μm and 5 μm (Fig. 1). This result occurred due to the mixing of two different size distributions, as described in Section 3, which improves particle packing.

The glass-vapor surface energy (γ) calculated by the SciGlass™ software was 0.334 J/m^2.

The viscosity curve was obtained by fitting the Vogel–Fulcher–Tamman equation ($\log(\eta) = A + B/(T - T_0)$) to both low- and high-viscosity data. The fitting parameters were $A = -5.12$; $B = 9829.41$ K and $T_0 = 378.94$ K (viscosity in Pa·s). The measured viscosity and fitted curve are shown in Fig. 2. The surface of our LAS glass presented fast crystallization, which prevented the measurements of viscosity in the temperature range of measurable sintering (780 °C to 1000 °C). Thus, unfortunately, the lack of data in this temperature range may induce some imprecision into the fitted viscosity equation (VFT).

The viscosity at T_g (as measured by DSC) is typically between 10^{12} and $10^{12.5}$ Pa·s [43]. Extrapolating the fitted equation, the predicted viscosity at T_g (665 °C) is $10^{12.3}$ Pa·s, which falls within the expected range and thus corroborates the validity of the fitted equation.

The partially crystallized surfaces of monolithic samples treated at different temperatures are shown in Fig. 3. Similar micrographs were used to measure maximum crystal radii to estimate the crystal growth rates. The crystal morphology changes with temperature. At 850 °C, a circular shape is observed, while at higher temperatures two different morphologies can be observed: hexagonal and irregular octagonal. Fig. 4 shows the XRD patterns of LAS glass with polished surfaces that were heat-treated at different temperatures.

Fig. 5(a) shows the measured values of the maximum crystal radii for heat treatments at each temperature for different times. The crystal growth rate, U(T) and the fitted equation assuming a linear behavior for log U(T) *versus* 1/T (in this limited T range) are shown in Fig. 5(b).

The parameter N_s was measured by SEM using a total of 22 images similar to the one shown in Fig. 6. The regions in the images with pores and protuberances were not considered. The average value and standard deviation was $(6 \pm 1) \times 10^{12}$ crystals/m^2.

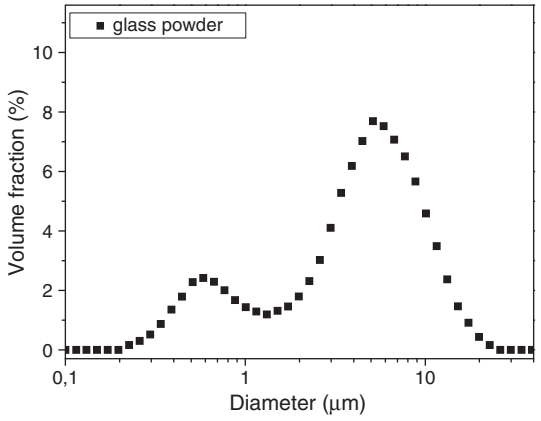

Fig. 1. Particle size distribution of the mixed glass powder before sintering.

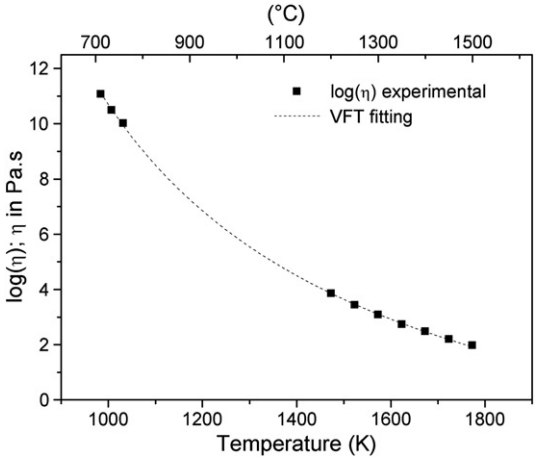

Fig. 2. Measured viscosity and VFT fitting of the experimental LAS glass.

4.2. Sintering and simulations

During the sintering process the sample partially crystallizes and its relative density should be calculated according to the true density of the body, which depends on the ratio between the volume of crystal and glass for each temperature. In this work the density goes a little over 1 because for simplicity we did not consider the effect of crystallization on the density of the sintered compact.

The parameters used for the simulation are listed in Table 1. We compared the model predictions to experimental data obtained from the tubular furnace (TF) and hot stage microscopy experiments (HSM). We considered that in the case of the small sample used in HSM there was no appreciable thermal gradient, so the model equation was fit to this curve and the adjustable parameter K_s determined to be 2, as shown in Fig. 7. Simultaneous sintering and surface crystallization can be observed in a broad temperature interval. However, in our experiments, almost full densification ($\rho = 98.5\%$) verified by optical microscopy was not hindered by concurrent crystallization. Using samples of 10 mm diameter heated in the TF, a displacement of about 16 to 20°C in relation to the HSM curve was observed.

The theoretical maximum crystal size as a function of temperature for a non-isothermal process was calculated considering unhindered growth, by $R_{MAX}(T) = \int_{T_0}^{T} \frac{U(T)}{q} dT$. A crystal diameter of 1.7 μm was calculated after sintering to 1000 °C. Fig. 8(a) shows the results for the temperature interval 700 °C–1000 °C. The actual crystals have a broad size distribution that depends on the glass particle size. Only crystals that nucleated on the surface of the largest particles have continuously grown toward their center until the end of the heat treatment, reaching the expected size. The finest particles were completely consumed by crystals at the beginning of the sintering process and hence these crystals were impeded to grow further. Fig. 8(b) shows the microstructure of a sintered sample (30 °C/min to 1000 °C) that illustrates this large size distribution of crystal radii, with crystal diameters always smaller than 1.7 μm, consistent with the simulation results.

5. Discussion

5.1. Crystal morphology

The different crystal morphologies observed in Fig. 3(d) are possibly associated with the existence of diverse crystalline phases. Glass-ceramics from the LAS system usually show a metastable β-quartz solid solution (virgilite ($Li_xAl_xSi_{3-x}O_6$)) at low temperatures that transforms into the stable β-spodumene solid solution (tetragonal keatite ss) at approximately 900 °C [44].

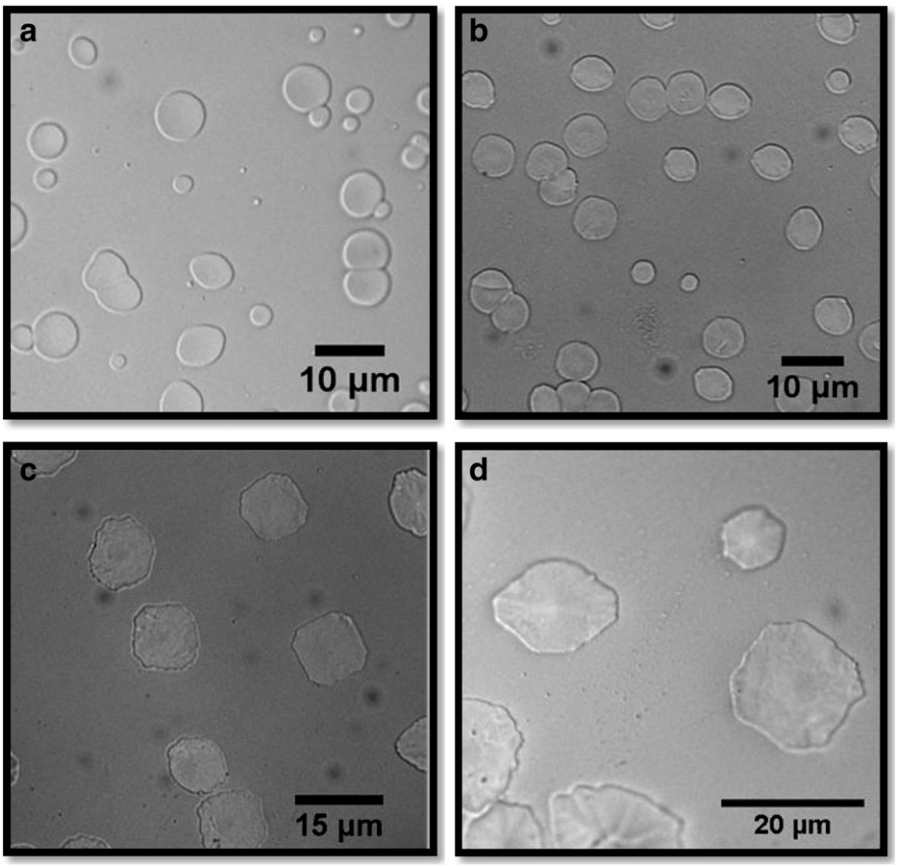

Fig. 3. Optical micrographs of the partially crystallized surfaces of monolithic samples treated at different temperatures and chemically etched in 2 vol.% HF: a) 850 °C — 161 min; b) 900 °C — 60 min; c) 950 °C — 45 min; d) 980 °C — 29 min.

We were interested in measuring the crystal growth rate of the metastable phase virgilite, but the time and temperature intervals used (850 °C to 980 °C) for heat treatments resulted in the simultaneous formation of β-spodumene (Fig. 4). In this work, it was not possible to identify if the change in crystal morphology was associated with the phase transformation of virgilite to β-spodumene. The largest crystal (among the regular octagons) was measured for each treatment time to determine crystal growth rates. Fig. 8 shows that the crystal radii predicted by the model using the measured U(T) agree with the experimental observations, which demonstrate the accuracy of U(T) for the considered temperature range.

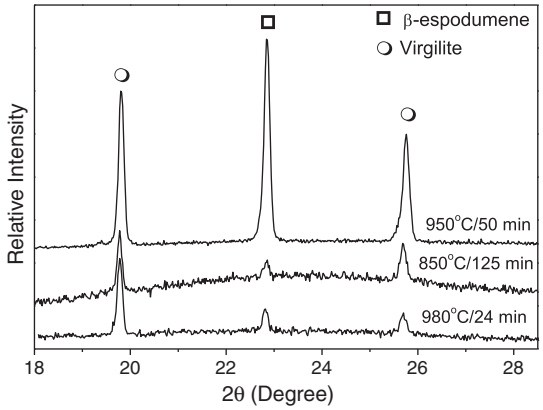

Fig. 4. XRD patterns of the partially crystallized surface of LAS glass heat-treated at different temperatures and times. Square: tetragonal β-spodumene ($LiAlSi_2O_6$) JCPDS 35-0794; and circles: hexagonal virgilite ($Li_xAl_xSi_{3-x}O_6$) JCPDS 31-0707.

5.2. Modified model

The difference between the solution to the MS model proposed by Prado et al. [24,25] and the solution proposed in this work depends on the crystallization kinetics of the glass. For that reason both versions of the model agree for the two extreme of crystallization: for the case in which there is no appreciable crystallization during sintering (full densification case) and for the case where the sample surface practically fully crystallizes before there is any sintering (no densification case).

For conditions in between these extremes, the solution proposed in this paper predicts a higher densification, which can reach about two percentage points (pp) in difference. This could, at least partially, explain previous results, where Prado et al. [25] calculated saturation densities about 2 pp lower than experimental results. Other important hypotheses for the limited agreement between theory and experiment raised in reference [25] are that glass–crystal and crystal–crystal interfaces have a different contribution to sintering than considered in the model and also the change of the residual glass composition – and thus viscosity – with crystallization.

5.3. Sintering and simulation

From our results calculated using Eq. (13) we have found that the relative saturation density reaches values somewhat greater than 1. The source of this inconsistency lies in the fact that we considered that the bulk density of the material remains constant for the whole process, ignoring the density changing effect of crystallization. But the density of the parent glass is 2.40 g/cm^3 while a sample sintered to 1000 °C actually reaches a density of 2.456 g/cm^3, which is very close to the density of the crystalline phase formed during sintering,

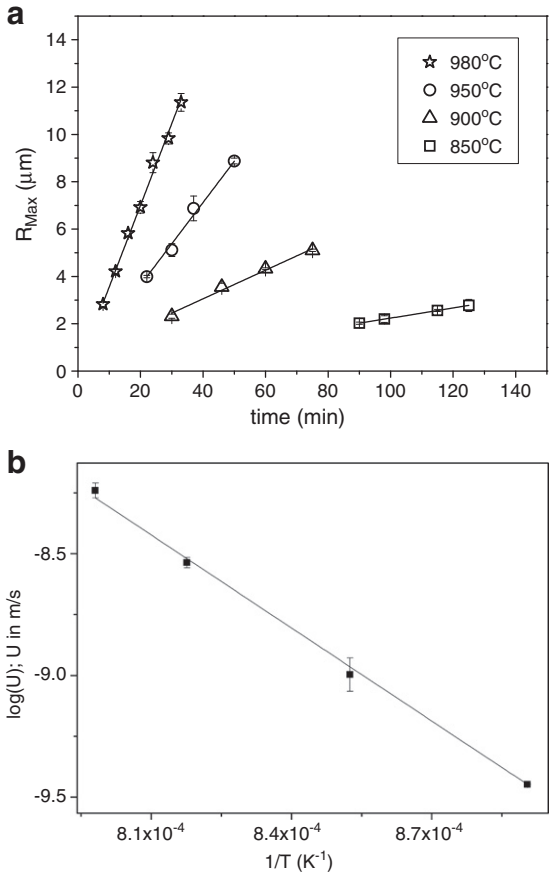

Fig. 5. Crystal growth data: a) measured maximum radii *versus* time for only one crystal morphology (approximately square or octagon); b) crystal growth rates for the LAS glass.

virgilite (2.46 g/cm^3). In a previous work, the crystalline volume fraction of virgilite was estimated from Rietveld refinement of a 1–1 mixture by weight of alumina and a sintered glass-ceramic powder. We found 84.1 ± 0.3% of virgilite, 4.6 ± 0.2% of an extra crystalline phase attributed to β-spodumene and 11% of a residual glassy phase [45]. We can estimate a lower bound for our densification experiments by assuming that at 1000 °C the glass ceramic is completely crystallized ($\rho = 2.46$ g/cm^3). The relative saturation density in the TF experiment reaches a value quite close to 1 and agrees to simulation, while in the HSM experiment it reaches 0.985. We consider the HSM results to be more accurate due to large errors associated with the geometrical method used to determine the density in the TF experiments. It is unusual to reach a densification of 100% in practice, even for non-crystallizing glasses and this is often associated to trapped insoluble gases inside the closed pores.

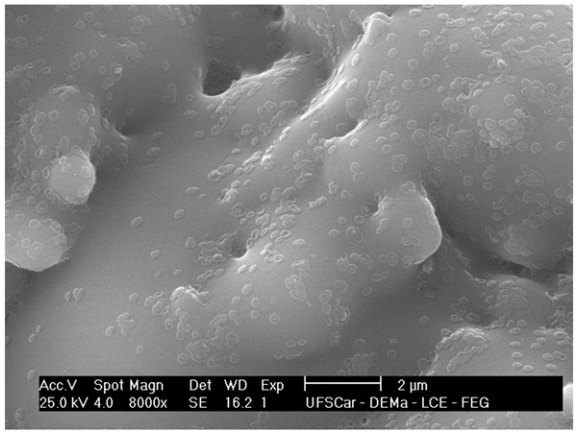

Fig. 6. SEM micrograph of an etched surface from a partially sintered compact treated to 900 °C using a heating rate of 30 °C/min. Several crystals can be observed growing on the surface of the glass particles.

Table 1
Parameters used for simulating the non-isothermal sintering process.

Parameters	Values
log (U(T)); U in m/s	2.104–12,989.88 K/T valid between 850 °C and 980 °C
log (η(T)); η in Pa·s	−5.12 + 9829.41 K/(T − 378.94 K)
N_s (sites/m^2)	6.0×10^{12}
γ (N/m)	0.334
ρ_0/ρ_g	0.68
Heating rate (q) (°C/min)	28
K_s	Fitting parameter range 1–5

5.4. Thermal gradients

Due to the low thermal conductivity of LAS and other glasses, thermal gradients across the specimens are an inconvenient implication of non-isothermal heat treatments of glasses, especially in large porous samples.

Prado et al. [25] estimated the temperature gradient within a glass compact cylinder of 10 mm of diameter. They found that the temperature difference between the sample surface and its central axis ($\Delta T = T_{surface} - T_{axis}$) was 4 K for a heating rate of 5 °C/min.

In this work, using a heating rate of 28 °C/min we expect a considerable larger value for ΔT. Indeed we found a temperature shift of about 16 °C to 20 °C in the sintering curves of 10 mm cylindrical samples in relation to almost cubic, ~33 mm^3 samples. The thermal gradient was efficiently minimized for the smaller sample and is likely to be responsible for the better agreement between the HSM data and simulation.

Here we choose not to estimate the thermal gradients since it is very hard to determine their exact magnitude due to large uncertainties in several parameters, such as the thermal conductivity of the compact as a function of porosity and temperature, the heat transfer coefficient for convection and the emissivity of surfaces for radiation.

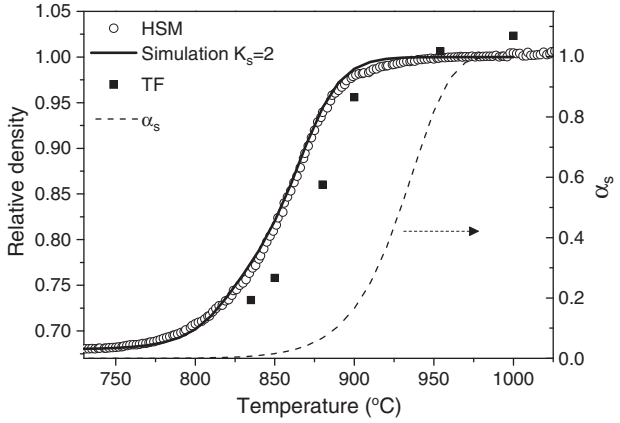

Fig. 7. Simulated densification curve *versus* temperature and experimental data for a heating rate of 28 °C/min. White circles correspond to hot stage microscope (HSM) data; and squares correspond to data obtained in tubular furnace (TF) considering the glass density (2.40 g/cm^3). The dashed curve shows the calculated evolution of surface crystallized fraction (α_s).

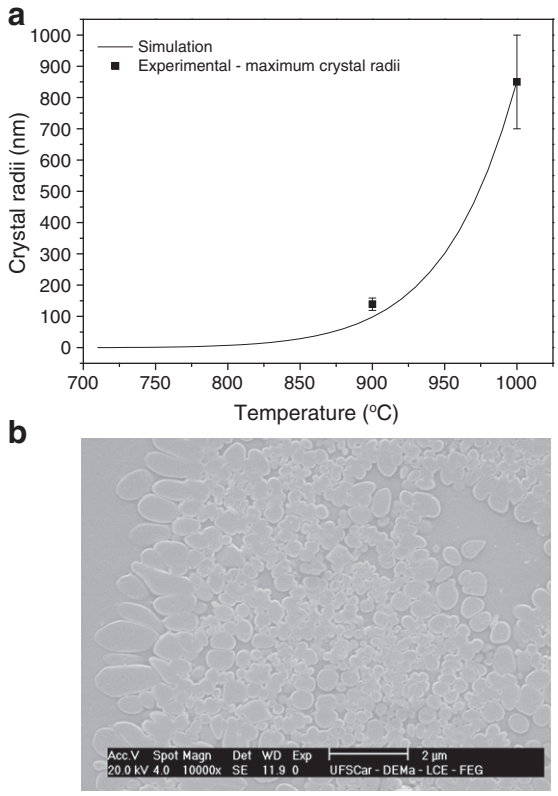

Fig. 8. Crystal radii predicted by simulation compared to those from the sample microstructure. a) Crystal radii as a function of temperature predicted by simulation using a heating rate of 28 °C/min. b) SEM micrograph of a polished and etched surface of LAS glass-ceramic sintered at 30 °C/min up to 1000 °C.

5.5. Effective viscosity (compositional and physical effects)

We assume that the viscosity of the parent glass controls the sintering process with concurrent crystallization. However, the effective viscosity of the compact changes with time due to crystallization for two reasons: i) the non-stoichiometry of the original glass, which causes continuous compositional changes of the glass matrix during crystallization and ii) the presence of crystals at the particle surface, which hinders viscous flow.

Crystallization of β-quartz$_{ss}$ (virgilite) in a non-stoichiometric multi-component glass preferentially consumes some ions (especially Li^+, Si^{4+}, O^{2-}, Al^{3+}) and some Mg^{2+} and Zn^{2+} of the glass and significantly changes the composition of the residual glass. Compared to virgilite, the parent glass is poorer in alkalis and has an excess of Al_2O_3. During crystallization, the diffusion of alkalis and SiO_2 to form crystals causes the residual glass to become enriched in Al_2O_3. This compositional change of the residual glass probably increases its viscosity during the sinter-crystallization process. The overall viscosity is also modified by the presence of solid inclusions (crystals). Müller et al. [46] showed that the effective viscosity of borosilicate glass increases with an increased volume fraction of alumina particles. Similarly, we expect that the effective viscosity of the compact continuously increases with crystallization during the sintering process.

In the *Clusters* model, the viscosity change during sintering with concurrent crystallization is not taken into account. For this reason, we do not expect that the experimental data will perfectly fit to the simulations for the temperature interval where crystallization and compositional changes are significant ($T > 800$ °C).

6. Conclusions

We have altered the solution of the non-isothermal MS equation in the *Clusters* model and have tested the modified model for a case of non-isothermal sintering with concurrent crystallization. A complex case of non-stoichiometric glass with a broad size distribution of jagged particles was sintered at a constant heating rate. Despite the complexity of the problem and the simplifying assumptions, we found good agreement between the experimental densification and the model's calculations using only one adjustable parameter (K_s).

The model assumes a homogeneous sample temperature during sintering. However, for relatively large porous samples and high heating rates, temperature gradients inside the sample must be considered. We found a mismatch of approximately 16–20 °C between the experimental and simulated densification data for 10 mm cylindrical compacts and a heating rate of 28 °C/min. For a significantly smaller sample, this temperature mismatch was not observed.

The proposed new algorithm thus provides a useful simulation tool to analyze or design the non-isothermal sintering of real glass powders with non-stoichiometric compositions that undergo simultaneous surface crystallization.

Acknowledgements

We thank FAPESP (07/08179-9; 2010/18947-6) and CNPq (Processes ANPCYT 490634/2008-7 and 143040/2008-1) for their financial support of this research project. We are also grateful to Oscar Peitl (São Carlos, Brazil) for the penetration viscosity measurements. Finally, we thank Dr. Miguel O. Prado (Bariloche, Argentina) for his critical comments.

References

[1] P.W. McMilan, Glass Ceramics, Academic Press, London, 1979.
[2] W. Hölland, G. Beall, Glass-Ceramic Technology, American Ceramic Society, Westerville, Ohio, 2002.
[3] W. Pannhorst, Recent developments for commercial applications of low expansion glass ceramics, Glass Technol. 45 (2004) 51–53.
[4] D. Krause, H. Bach, Low Thermal Expansion Glass Ceramics, second ed. Springer-Verlag, Berlin, Heidelberg, New York, 2005.
[5] E.D. Zanotto, A bright future for glass-ceramics, Am. Ceram. Soc. Bull. 89 (8) (2010) 19–27.
[6] U. Schiffner, Nucleation in parent glasses for lithia alumino-silicate glass-ceramics, in: H. Bach, D. Krause (Eds.), Low Thermal Expansion Glass Ceramics, 2 Edition, Springer, Berlin/Heidelberg/New York, 2005, pp. 25–39.
[7] P. Riello, P. Canton, N. Comelato, S. Polizzi, M. Verità, G. Fagherazzi, H. Hofmeister, S. Hopfe, Nucleation and crystallization behavior of glass-ceramic materials in the Li_2O–Al_2O_3–SiO_2 system of interest for their transparency properties, J. Non-Cryst. Solids 288 (2001) 127–139.
[8] D.R. Stewart, in: L.L. Hench, S.W. Freiman (Eds.), Advances in Nucleation and Crystallization of Glasses, Symposium Glass DivisionAmerican Ceramic Society, Columbus, Ohio, 1971, p. 83.
[9] A.W.A. El-Shennawi, A.A. Omar, A.M. Morsy, The role of titania and titania mixtures in the nucleation and crystallization of spodumene–willemite–diopside glasses, Thermochim. Acta 58 (2) (1982) 125–153.
[10] E.M. Rabinovich, Review: preparation of glass by sintering, J. Mater. Sci. 20 (1985) 4259–4297.
[11] E.M. Rabinovich, in: J.H. Simmons, D.R. Uhlmann, G.H. Beall (Eds.), Nucleation and Crystallization in Glasses, Advances in Ceramics, vol. 4, American Ceramic Society, Columbus Ohio, 1982, pp. 327–333.
[12] R. Müller, E.D. Zanotto, V.M. Fokin, Surface crystallization of silicate glasses: nucleation sites and kinetics, J. Non-Cryst. Solids 274 (1–3) (2000) 208–231.
[13] T.J. Clark, S.J. Reed, Kinectic process involved in the sintering and crystallization of glass powder, J. Am. Ceram. Soc. 69 (11) (1986) 837–846.
[14] E.I. Suzdal'tsev, D.V. Kharitonov, Intensified sintering of lithium aluminosilicate ceramics, Refract. Ind. Ceram. 2 (2004) 88–90.
[15] S. Knickerbocker, M.R. Tuzzolo, S. Lawhorne, Sinterable β-spodumene glass-ceramics, J. Am. Ceram. Soc. 72 (10) (1989) 1873–1879.
[16] Y.M. Sung, Mechanical properties of α-cordierite and β-spodumene glass-ceramics prepared by sintering and crystallization heat treatments, Ceram. Int. 23 (1997) 401–407.
[17] Y.M. Sung, S.A. Dunn, J.A. Koutsky, The effect of boria and titania addition on the crystallization and sintering behavior of Li_2O–Al_2O_3–$4SiO_2$ glass, J. Eur. Ceram. Soc. 14 (1994) 455–462.
[18] M.C. Wang, S. Yang, S.B. Wen, N.C.Wu. Sintering, Li_2O–Al_2O_3–$4SiO_2$ precursor powders with ultrafine TiO_2 additives, Mater. Chem. Phys. 76 (2002) 162–170.

[19] M.C. Wang, N.C. Wu, S. Yang, S.B. Wen, Morphology and microstructure in the sintering of β-spodumene precursor powders with TiO_2 additive, J. Eur. Ceram. Soc. 23 (2003) 437–443.
[20] M. Guedes, A.C. Ferro, J.M.F. Ferreira, Nucleation and crystal growth in commercial LAS compositions, J. Eur. Ceram. Soc. 21 (9) (2001) 1187–1194.
[21] P. Riello, S. Bucella, L. Zamengo, U. Anselme-Tamburini, R. Francini, S. Pietrantoni, Z.A. Munir, Erbium-doped LAS glass-ceramics prepared by spark plasma sintering (SPS), J. Eur. Ceram. Soc. 26 (2006) 3301–3306.
[22] E.I. Suzdal'tsev, D.V. Kharitonov, Intensified sintering of lithiumaluminosilicate ceramics, Refract. Ind. Ceram. 45 (2) (2004) 88–90.
[23] E.I. Suzdal'tsev, Effect of temperature on the structuring and properties of glass and glass ceramic of lithium aluminosilicate composition, Refract. Ind. Ceram. 43 (3–4) (2002) 127–135.
[24] M.O. Prado, C. Fredericci, E.D. Zanotto, Glass sintering with concurrent crystallization.Part 2.Nonisothermal sintering of jagged polydispersed particles, Phys. Chem. Glasses 43 (5) (2002) 215–223.
[25] M.O. Prado, C. Fredericci, E.D. Zanotto, Non-isothermal sintering with concurrent crystallization of polydispersed soda–lime–silica glass beads, J. Non-Cryst. Solids 331 (2003) 157–167.
[26] M.O. Prado, E.D. Zanotto, R. Müller, Model for sintering polydispersed glass particles, J. Non-Cryst. Solids 279 (2001) 169–178.
[27] E.D. Zanotto, M.O. Prado, Isothermal sintering with concurrent crystallization of monodispersed and polydispersed glass particles, Phys. Chem. Glasses 42 (3) (2001) 191–198.
[28] M.O. Prado, E.D. Zanotto, Glass sintering with concurrent crystallization, C.R. Chim. 5 (2002) 773–786.
[29] M.O. Prado, E.D. Zanotto, C. Fredericci, Sintering polydispersed spherical glass particles, J. Mater. Res. 18 (6) (2003) 1347–1354.
[30] M.O. Prado, C. Fredericci, E.D. Zanotto, Isothermal sintering with concurrent crystallization of polydispersed soda–lime–silica glass beads, J. Non-Cryst. Solids 331 (2003) 145–156.
[31] M.O. Prado, E.B. Ferreira, E.D. Zanotto, Sintering kinetics of crystallizing glass particles. A review, in: Hong Li, Chandra S. Ray, Denis M. Strachan, Richard Weber, Yuanzheng Yue (Eds.), Ceramic Transactions — Melt Chemistry, Relaxation, and Solidification Kinetics of Glasses, The American Ceramic Society, Westerville, 2005, pp. 63–180, 170.
[32] J. Frenkel, Viscous flow of crystalline bodies under the action of surface tension, J. Phys. (USSR) 9 (5) (1945) 385.
[33] J.K. Mackenzie, R. Schuttleworth, A phenomenological theory of sintering, Proc. Phys. Soc. London, Sect. B 62 (1949) 833.
[34] C. Lara, M.J. Pascual, M.O. Prado, A. Durán, Sintering of glasses in the system RO–Al2O3–BaO–SiO2 (R = Ca, Mg–Zn) studied by hot-stage microscopy, Solid State Ionics 170 (2004) 201–208.
[35] M.C. Weinberg, Surface nucleated transformation kinetics in 2- and 3-dimensional finite systems, J. Non-Cryst. Solids 134 (1991) 116–122.
[36] R. Müller, M. Kirsch, H. Lorenz, Surface crystallization a limiting effect of sintering glass powders, in: 15th Congress on Glass, Leningrad, 3, 1989, p. 334.
[37] M.J. Pascual, A. Durán, Sintering with concurrent crystallisation of a borosilicate glass, Phys. Chem. Glasses 44 (6) (2003) 409–415.
[38] M.J. Pascual, A. Durán, M.O. Prado, E.D. Zanotto, Model for sintering devitrifing glass particles with embedded rigid fibers, J. Am. Ceram. Soc. 88 (6) (2005) 1427–1434.
[39] D.S. Rodriguez, G. Mosca, M.O. Prado, The sintering rate of glass powders, in: 9th International Symposium on Crystallization in Glasses and Liquids, Foz do Iguaçú, Brazil, 2009.
[40] J.E. Funk, D.R. Dinger, Particle packing, part 1 — fundamentals of particle packing monodisperse spheres, Interceram 41 (1) (1992) 10–14.
[41] R.G. Pileggi, F. Ortega, R. Morábito, S. Vendrasco, V.C. Pandolfelli, Development and application of a software designed to combine different raw materials in order to obtain ceramic products, Cerâmica 44 (289) (1998) 189–195.
[42] V.O. Soares. Synthesis of Li_2O–Al_2O_3–SiO_2 (LAS) glass-ceramics by sintering with concurrent crystallization. MScDissertation (Master'sdegree in MaterialsScience and Engineering), Federal University of São Carlos, Brazil 2007. (in Portuguese).
[43] J.M.F. Navarro, El Vídrio, Third ed. Artegraf, Madrid, 2003. 314–334.
[44] R. Wurth, F. Muñoz, M. Müller, C. Rüssel, Crystal growth in a multicomponent lithia aluminosilicate glass, Mater. Chem. Phys. 116 (2009) 433–437.
[45] F.C. Serbena, V.O. Soares, O. Peitl Filho, H. Pinto, R. Muccillo, E.D. Zanotto, Internal residual stresses in sintered and commercial low expansion Li_2O–Al_2O_3–SiO_2 glass-ceramics, J. Am. Ceram. Soc. 94 (4) (2011) 1206–1214.
[46] R. Müller, M. Eberstein, S. Reinsch, W.A. Schiller, J. Deubener, A. Thiel, Effect of rigid inclusions on sintering of low temperature co-fired ceramics, Phys. Chem. Glasses Eur. J. Glass Sci. Technol. B 48 (4) (2007) 259–266.